Article

A Blended SPS-ESPS Control DAB-IBDC Converter for a Standalone Solar Power System

P. Sathishkumar [1], Himanshu [1], Shengxu Piao [1], Muhammad Adil Khan [1], Do-Hyun Kim [1], Min-Soo Kim [1], Dong-Keun Jeong [2], Cheewoo Lee [3] and Hee-Je Kim [1,*]

[1] School of Electrical Engineering, Pusan National University, Busandaehak-ro 63 beon-gil 2, Busan 46241, Korea; sathishnano2013@gmail.com (P.S.); himanshuhimanshu820@gmail.com (H.); piaoshengxu88@hotmail.com (S.P.); engradilee@gmail.com (M.A.K.); kdh8486@naver.com (D.-H.K.); rlaalstn5122@naver.com (M.-S.K.)

[2] Power Conversion and Control Research Centre, HVDC Research Division, KERI, Changwon 51435, Korea; keunygajjang@nate.com

[3] School of Electrical Engineering, Pusan National University, Busan 46241, Korea; cwlee1014@pusan.ac.kr

* Correspondence: heeje@pusan.ac.kr; Tel.: +82-51-510-2364

Abstract: In sustainable energy applications, standalone solar power systems are mostly preferred for self-powered energy zones. In all standalone renewable power systems, batteries are still preferred as the common energy storage device. On the other hand, batteries are not applicable for high peak power demand applications because of their low power density. A supercapacitor is a preferable high-power density energy storage device for high peak power applications. A 2 kW, 50 kHz digital control dual active bridge isolated bi-directional dc-dc converter (DAB-IBDC) was developed for interfacing the supercapacitor bank in standalone solar power system. This paper proposes a blended SPS-ESPS digital control algorithm for a DAB-IBDC converter instead of using a traditional single-phase shift (SPS) control algorithm, which is commonly used for large input to output voltage varying applications. This proposed blended SPS-ESPS control algorithm achieved high power conversion efficiency during a large input to output voltage variation, over a traditional phase shift control algorithm by reducing the back-power flow and current stress in a circuit. This system also achieved maximum power point for solar modules and enhanced rapid charging-discharging for a supercapacitor bank. Both SPS and the blended SPS-ESPS control algorithms were verified experimentally using 2 kW DAB-IBDC topology implemented with standalone power system that combination of 2000 W input solar module and 158 Wh supercapacitor bank.

Keywords: dual active bridge; isolated bi-directional dc-dc converter; DAB-IBDC; blended SPS-ESPS; high power density energy storage system; standalone solar power system

1. Introduction

Over the last decade, fossil fuel technology has become less attractive due to the depletion of reserves on Earth. Renewable energy sources are believed to be an alternative energy source to replace fossil fuels. Among renewable energy systems, stand-alone photovoltaic systems are commonly preferred in remote areas. A typical stand-alone system incorporates a photovoltaic panel, maximum power point tracker (MPPT), energy storage system, and charging controller [1]. A photovoltaic system is not an ideal dc source for charging energy storage systems gradually because it does not satisfy the desirable requirements of storage devices. The output of such a system is dependent on the frequent changeable weather conditions, which are largely unpredictable. Therefore, the photovoltaic system output is unreliable and the optimal charge and discharge cycle cannot be guaranteed [2]. With lead acid batteries, which are the most prefer common energy storage device in standalone

renewable energy systems, this unreliable charging results in a low battery state of charge, which leads to sulphating and stratification that both shorten battery life cycle [3]. To avoid this, a MPPT and charge controller are used as an intermediate circuit in a renewable solar energy system between the solar source and energy storage device.

Recently, researchers have focused on supercapacitors as an energy storage device instead of using batteries. Supercapacitors have several advantages over batteries, such as the ability to handle high peak power, high power density, instantaneous turn on ability, and rapid charge-discharge capability. These unique properties of a supercapacitor make it ideal energy storage device in certain load applications where high peak power demand is necessary. For example, in motor starting applications, the starting current requirement can be 6–10 times higher than the normal operating current of the motor. Electric vehicles are likely to employ electrically powered actuators for high-power transient loads. A supercapacitor-based energy storage system has been proposed to meet the peak power demands of the electric vehicle loads and absorb the regenerated power [4,5]. On the other hand, the major limitation of supercapacitors is their lower energy density, so they cannot store large amounts of energy like a battery. For example, if a supercapacitor is to be used to store the same energy as a lead acid battery, with the present technology, the supercapacitor must be ten times larger than the corresponding battery. Although large size is considered a major disadvantage of a supercapacitor, it can still be applied in an energy storage system because of its higher power density. Many studies of the material side have attempted to improve the supercapacitor energy density towards to make it an efficient energy storage device [6]. In future, the energy density of supercapacitors will hopefully be much improved compared to conventional batteries. Nowadays, lead acid batteries with solar source are commonly used for developing self-powered energy zones commonly known as no-power grid zones. Although lead acid batteries are appropriate for self-powered energy zones, however while handling high peak power appliances such as air-conditioners, mixers, grinders, etc. the current stress on the batteries is increased enormously which leads batteries to be badly damaged. Many researchers have proposed supercapacitors or combinations of supercapacitors and batteries as energy storage devices in stand-alone power systems for developing a better self-powered energy zone [5].

Many dc-dc converter topology and control approaches are being proposed in standalone renewable energy storage systems for achieving maximum power, high power conversion efficiency and secure fast charging-discharging [7–10]. In the design of high power dc-dc converters, the main trade-offs are between the power efficiency and power converter. Since the 1970s, the power semiconductor technology has been developed, resulting in a significant increase in the power density of power electronic converters. With more progressive power semiconductor devices, switch mode power electronic converters with a higher switching frequency have been developed. Therefore, the volumes of the converter circuits can be decreased. Power semiconductors and integrated circuits have been developed to economically produce dc-dc converters.

Based on reviews, among all the dc-dc converters for interfacing renewable sources and high-power density-energy storage devices, because of its unique characteristics a Dual Active Bridge-Isolated Bidirectional DC-DC Converter (DAB-IBDC) was proposed by the authors in the early 1990s [11]. On the other hand, because of the performance limitations of power devices, the power losses of DAB-IBDC were high and the efficiency was unacceptable. In recent years, the advances in new power devices and magnetic materials have made DAB-IBDC a simple and low loss converter circuit among all other converters [12]. For power conversion, the DAB-IBDC topology is popular among researchers because of its high performance, high efficiency, galvanic isolation, ability for handling high power density, both side power flow ability, and inherent soft switching property. These features make the DAB-IBDC a typical circuit for high power density applications [13]. Several papers have been published and the performance and comprehensive analyses of DAB converters have been reported.

Design considerations of the DAB converter and high frequency DAB transformer were discussed briefly under the assumption of future trends [14]. Nayagi et al. proposed a new model for the steady

state analysis of a DAB converter circuit that produces equations for rms and average device currents, and rms and peak inductor currents. These equations are useful for predicting the losses that occur in the device and passive components [15]. A previous study [16] optimized the design of a dual active bridge converter permitting flexible interfacing to energy storage devices to achieve uninterrupted power supply in military applications. The DAB performance for the next generation power conversion systems using ultra-capacitor-based technologies has been validated [17]. The performance of an ultra-capacitor-based DAB converter dynamic was modelled and analyzed [18]. According to previous research based on a digital control algorithm, ESPS control of an isolated bi-directional dc-dc converter is improving the system efficiency of the circuit for power distribution between the energy source and energy storage system in micro grids over a wide input voltage and output power range [19]. The current stress and backflow power of an isolated converter circuit was analyzed using ESPS control and it was verified that ESPS achieves greater efficiency with an inner phase limitation over SPS control under microgrid applications [20].

This paper proposes a modified digital control DAB-IBDC converter to be deployed in a standalone solar power system coupled with a high-power density energy storage device, as shown in Figure 1. The proposed algorithm can operate the solar source at its maximum power point (MPPT), converting power with the maximum conversion efficiency and enhancing the rapid charging-discharging for high power density energy storage devices. In the digital control algorithm, the blended SPS-ESPS control algorithm operates a converter with the maximum power conversion efficiency by reducing the back-flow power in a converter circuit. In such large voltage varying applications ($k > 1$) like a renewable energy source, the back-flow power of a DAB-IBDC converter is large, which leads to an increase in the current stress in a circuit. Therefore, the overall circuit performance will be affected and the power conversion efficiency will be reduced. The proposed blended SPS-ESPS digital control algorithm continuously monitors the back-power flow in a circuit and reduces it as much as possible by adjusting the inner phase shift of the primary bridge. In this laboratory, 2 kW DAB-IBDC topology with MOSFET switching bridges was developed. The overall control algorithm was verified experimentally using this topology in a 2000 W standalone solar power system. To analyses the modified control algorithm, the experiment was also conducted using the traditional single-phase shift (SPS) algorithm. The results are discussed based on the experimental results and it was concluded that the proposed blended SPS-ESPS digital control DAB-IBDC converter gains more efficiency over traditional phase shift DAB converters. The results showed that the blended SPS-ESPS digital control DAB-IBDC is more suitable for a standalone renewable power system in high peak power demand applications, such as electric vehicles, motors, etc.
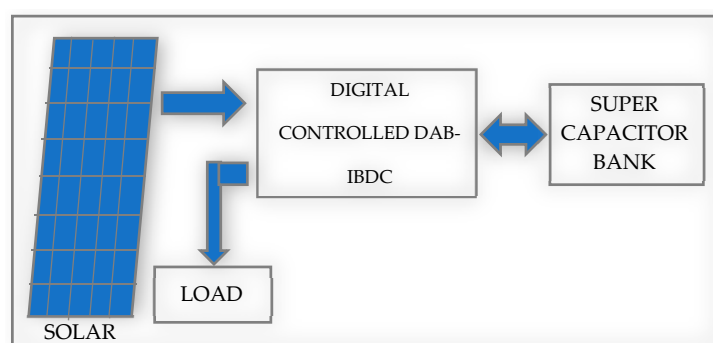

Figure 1. Block diagram of a standalone photovoltaic power system.

2. DAB-IBDC Converter Circuit

Figure 2 presents a schematic diagram of the digital control dual active bridge−isolated bidirectional dc-dc converter circuits. These circuits are simply structured with two full bridges isolated by a high frequency high power transformer. Both side power flow exists in a circuit and is controlled by the DSP controller (TMS320F28335, Texas Instruments, Dallas, TX, USA). The schematic diagram explanation, principle of operation, and steady state model of a circuit are explained below.
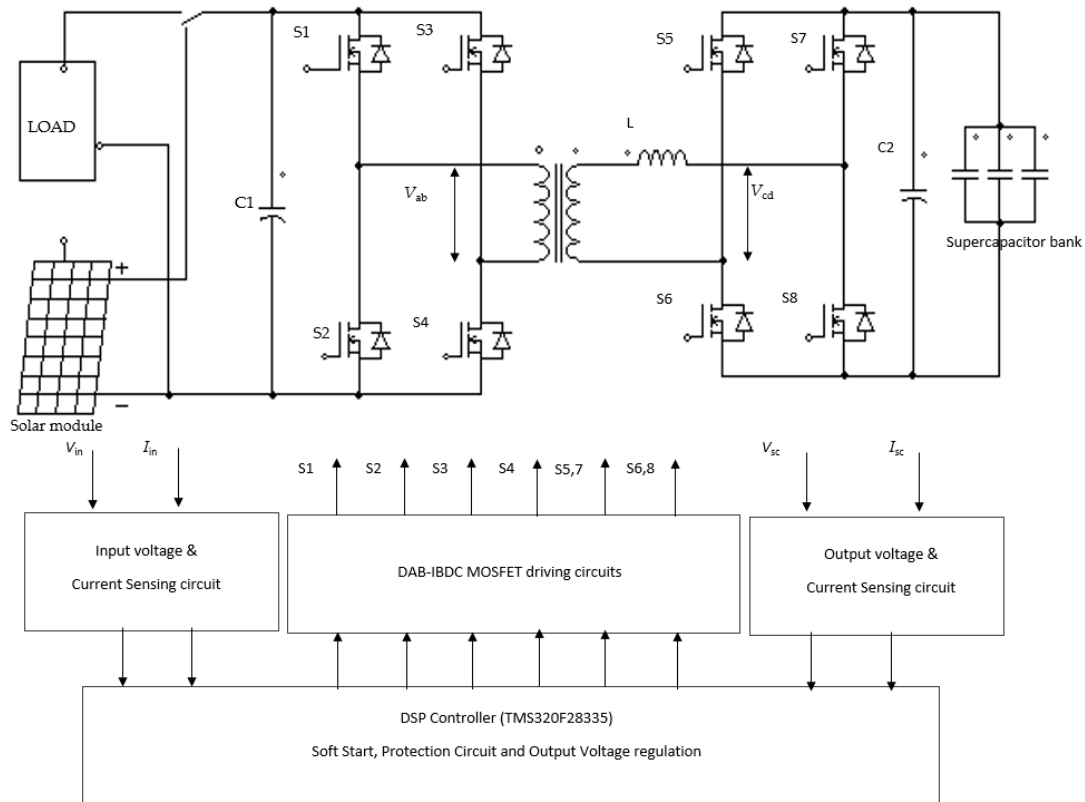

Figure 2. Schematic diagram of Digital Controlled Dual Active Bridge-Isolated Bidirectional DC-DC Converter (DAB-IBDC).

A Dual Active Bridge converter contains an isolated transformer with a leakage Inductance, L_{leq}. The required inductance for the circuit is provided partly or entirely by the transformer leakage inductance. If needed, an additional coupling inductor may be connected in series with the transformer leakage inductor to boost the overall inductance of the converter circuit based on the conversion requirements. The isolated transformer isolates the two full-bridge circuits, in that the primary side full bridge is connected to a high voltage DC source called a high voltage bridge (V_{ab}) and another full bridge on the secondary side is connected to a low voltage energy storage system called a low voltage bridge (V_{cd}). In forward mode, the current flows from the source to the supercapacitor until the supercapacitor is charged fully. The load is connected to the primary side of the circuit because it can be powered up by the energy storage system in the backward mode of operation. Both side full bridges consist of four 47N60C3 MOSFETs (Infineon Technologies, Hong Kong, China), as shown in Figure 2, and are controlled by a high frequency square wave voltage given by the DSP followed by a MOSFET driver. Both side bridges, two square waves can be suitably phase shifted with respect to each other to control the power flow direction. In forward mode, the phase of the V_{cd} square wave is shifted by the V_{ab} square wave. In contrast, in backward mode, the phase of the V_{ab} square wave is shifted by the phase of the V_{cd} square wave. Therefore, bidirectional power flow is enabled in a DAB

converter. The current flow occurs because of the voltage difference across the inductor due to the phase shift between these two bridges square wave voltages.

In Figure 3, L is the sum of the transformer leakage inductance, L_{leq}, and coupling auxiliary inductance L_1. V_{ab} and V_{cd} are the equivalent AC output voltages of primary and secondary side, respectively. V_L and I_L are the voltage and current of the inductor, L. The power-flow direction and magnitude of power can be controlled simply by adjusting the phase shift between V_{ab} and V_{cd}. Although various digital control algorithms were proposed, the traditional single-phase shift (SPS) algorithm is still preferred by many researchers for its unique characteristics such as high power handling ability and handling large input to output voltage variation [2]. Extended single-phase shift control (ESPS) is preferred by researchers to increase the conversion efficiency by reducing the back-power flow and current stress in a circuit. Regarding increasing conversion efficiency, compared to other digital control algorithms it can be implemented very easily by adding an inner phase shift at the primary side bridge. Both the control algorithm and forward mode waveform shown in the Figure 4 were assessed by waveform steady state analysis.
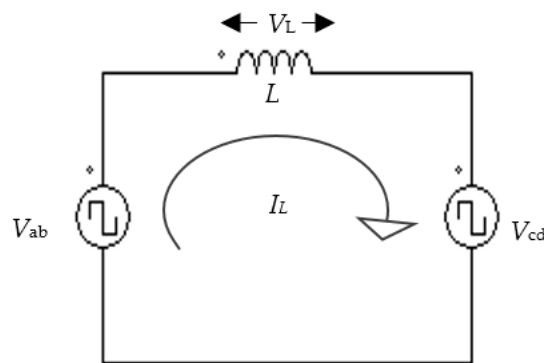

Figure 3. Equivalent circuit of phase-shift control.

Steady State Analysis

Figure 4 shows the main waveforms of DAB-IBDC in SPS and ESPS control, where T_{hs} is a half switching period, and d is the phase-shift ratio between the primary and secondary voltages of the isolation high frequency transformer, where $0 \leq d \leq 1$. In Figure 4a V_{ab} and V_{cd} are both square wave voltages and the interaction between these two voltages occurred through the inductor of the circuit. Therefore, the primary voltage is always in the miss-phase with the primary current because it passes through the inductor. The average currents of the leakage inductor are derived based on the waveform I_L. The difference in voltage between V_{ab} and V_{cd} appears across the inductor, L, and inductor current, I_L, at the switching instants, t_1 and t_2, respectively:

$$I_p = \frac{T_s}{4L}[nV_{in} + V_0(2d - 1)] \tag{1}$$

$$L_1 = \frac{T_s}{4L}[nV_{in}(2d - 1) + V_0] \tag{2}$$

The waveform is a periodic over a half cycle. Thus, dividing the area by the duration $T_s/2$, the average output current of the DAB converter:

$$I_0 = \frac{nV_{in}T_s}{2L}\left(d - d^2\right) \tag{3}$$

Normally the average output current depends on $\frac{nV_{in}T_s}{2L}$:

$$I_0' = \left(d - d^2\right) \tag{4}$$

From Equation (4), by substituting full control range 0–1 to the phase shift d, it can be observed that maximum power transfer occurs for a duty ratio of 0.5.
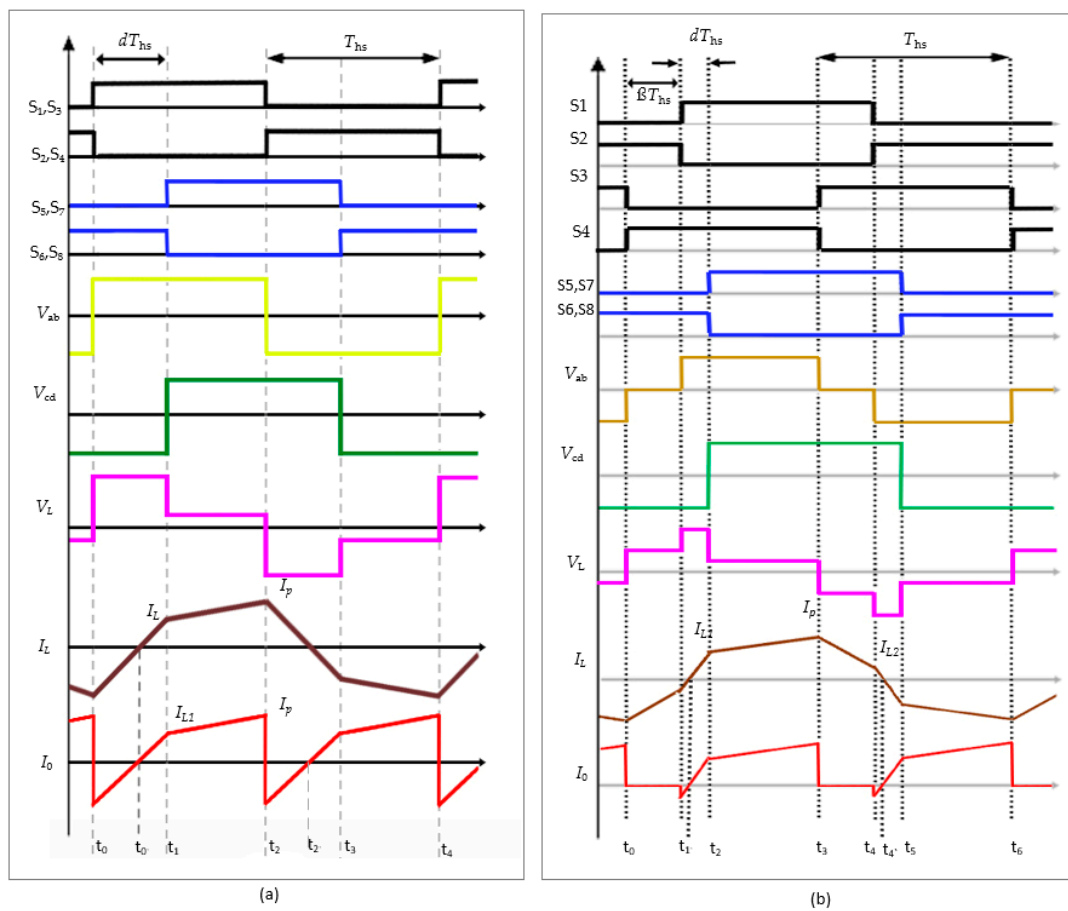

Figure 4. Key operating waveforms of DAB-IBDC during forward (buck) mode. (**a**) Traditional single-phase shift control (SPS); (**b**) extended phase shift control (ESPS).

As shown in Figure 4, I_L is of the opposite phase from V_{ab} for an interval of $t = t_0-t_0'$ and $t = t_2-t_2'$ is a portion of the power delivered to the V_{out} side in a single switching period. The other portion $t = t_0'-t_1$ and $t = t_2'-t_3$, is sent back to the primary voltage source, V_{in}. This is defined as backflow power for a given transmission power. The total transmission power and backflow power can be derived as follows:

$$P = \frac{n V_{in} V_{out} T_s}{2L} \left(d - d^2 \right) \tag{5}$$

$$P_{bf} = \frac{n V_{in} V_{out} T_s [k + (2d - 1)]^2}{16L(k + 1)} \tag{6}$$

where, n = Transformer turns ratio, k = Voltage transfer ratio, d—phase shift, V_{in} = input voltage, V_{out} = charging voltage, L = inductance of a converter, T_s = Switching time.

With increasing backflow power, the forward power also increases to compensate for the loss caused by backflow power. The circulating power and current stress are then increased, which result in great loss in power devices and magnetic components and low efficiency of the converter:

$$I_{max} = \frac{n V_2 T_s}{4L} (2d - 1 + k) \tag{7}$$

From Equations (1)–(7), maximum power transfer occurs at a duty ratio of 0.5. Even the same transfer power is achieved for a duty of 0.5–1, which is the same as 0 to 0.5, in that the backflow power and current stress will be low in a region where the duty is 0–0.5 compared to the duty 0.5–1 region.

To decrease the backflow power, V_{ab} should not be confined to a square wave with a 50% duty cycle. In figure, S_1 and S_4 have a phase shift of β, which reduces the V_{ab} square wave duty cycle. The transformer primary voltage will emerge as three levels instead of two levels in SPS control. This alters the behavior of the I_L current, as shown in the figure. The inductor current (I_L) changes in three instants of time t_2, t_3, and t_4, which are denoted as I_{L1}, I_P, and I_{L2}, respectively:

$$I_{L2} = \frac{T_s}{4L}[nV_{in}(1-\beta) + V_0(2d-1)] \tag{8}$$

$$I_{L1} = \frac{T_s}{4L}[nV_{in}(2d-1+\beta) + V_0] \tag{9}$$

$$I_p = \frac{T_s}{4L}[nV_{in}(1-\beta) + V_0(2d-1+2\beta)] \tag{10}$$

where, β = inner phase shift, d—outer phase shift, T_s = Switching time.

If see a waveform, it's a periodic over half cycle, dividing the area by the duration $T_s/2$, gives the average output current of the DAB converter is:

$$I_0 = \frac{nV_{in}T_s}{2L}[d - d^2 - dss + \frac{\beta}{2} - \frac{\beta^2}{2}] \tag{11}$$

Normalised the average output current based on the values $\frac{nV_{in}T_s}{2L}$ gives:

$$I_0' = d - d^2 - d\beta + \frac{\beta}{2} - \frac{\beta}{2} \tag{12}$$

the backflow power appearance time are divided into two intervals $t = t_0 – t_1$, $t = t_1 – t_1'$ and $t = t_3 – t_4$, $t = t_4 – t_4'$. The backflow power is zero as transformer primary voltage reaches zero for the first intervals. Thus, overall backflow power decreased for a given transmission power:

$$P' = \frac{1}{T_{hs}}\int_0^{T_{hs}} V_{h1}i_L(t)dt = \frac{nT_sV_1V_2}{2L}\left(d(1-d) + \frac{1}{2}\beta(1-\beta-2d)\right) \tag{13}$$

Backflow power:

$$P_{bf}' = \frac{1}{T_{hs}}\int_{t_1}^{t'_1} V_{h1}|i_L(t)|dt = \frac{nT_sV_1V_2[k(1-\beta) + (2d-1)]^2}{16L(k+1)} \tag{14}$$

where, k = voltage transfer ratio.

Current stress under ESPS control:

$$I'_{max} = \frac{nT_sV_2}{4L}(k(1-\beta) + (2\beta+2d-1)) \tag{15}$$

where $i_L(t_1) < 0$, from equation, we have

$$k > \frac{1-2d}{1-\beta} \tag{16}$$

When $k \le (1-2d)/(1-\beta)$, the back-power flow is zero.

In figure, β is the phase shift ratio between the driving signals of S1 & S4, and S2 & S3 in the primary bridge. β is defined as the inner phase shift ratio, where $0 \le \beta \le 1$. d is the phase shift ratio between the primary and secondary voltages of the isolation transformer. d is often known as the outer

phase shift ratio, where $0 \leq d \leq 1$ and $0 \leq \beta + d \leq 1$. Compared to the SPS control, ESPS control have not only an outer phase shift ratio, but also an inner phase shift ratio, which will decrease the current stress, expand the regulating range of transmission power, and enhance the regulating flexibility.

3. Experiments

Figure 5 presents the developed 2 kW DAB-IBDC converter circuit and experimental setup. In DAB-IBDC topology, both side active bridges have been designed with a 47N60C3 power MOSFET. The equivalent gate capacitance is expressed by the gate–source and gate–drain capacitors. The drain source resistance is 0.07 Ω, which is considered the best value among all other MOSFET switches. According to the datasheet, the drain source voltage is nearly 650 V and drain current is 47 A, pulsed drain current is 141 A. To trigger the MOSFET switches at a high frequency (f > 10 kHz), pulse width modulation (PWM) signals (±7 to ±30 V, 3 mA) need to be applied across the gate-source terminal.
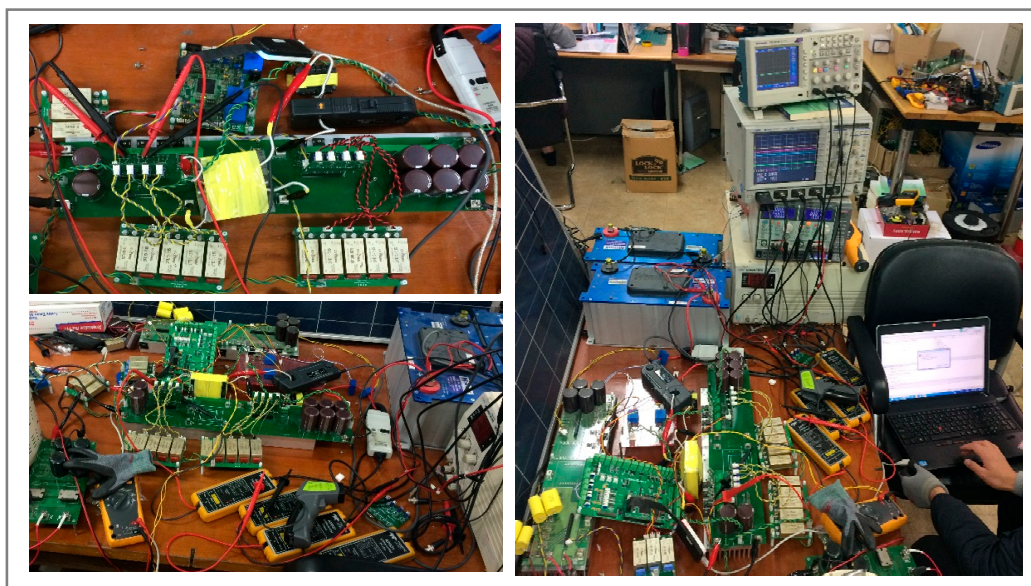

Figure 5. Developed DAB-IBDC converter and experimental setup.

The applied PWM signals are generated by digital signal processor (TMS320F28335) based on the control algorithm. As these PWM signals from DSP do not have sufficient power to operate switches, a MOSFET driving circuit was designed and used to interface the DSP and MOSFET switches. The driver circuit input and output waveform signal are shown in Figure 6. The designed MOSFET driver converts the low power 0 to 5 V PWM signal to a −3 to 12 V high power PWM signals, which can turn the switches on and off.
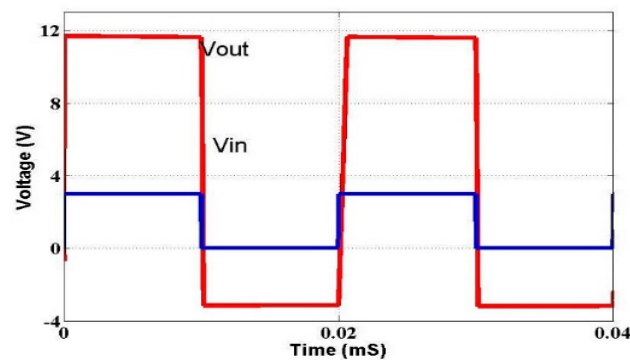

Figure 6. Input and output signal waveform of MOSFET driver circuit.

The previous power conversion system (PCS) is employed mainly with a line frequency (LF) transformer to achieve isolation and voltage matching. Basically, the LF transformer size is extremely large, which hinders the design of a simple PCS. In the LF transformer, current-voltage distortions and losses are high due to core saturation. Overall, in previous PCSs, the LF transformer reduces the power conversion efficiency and power density. With the aim of increasing the efficiency and power density of a converter, a high frequency power conversion system has recently been proposed. When the switching frequency is above 20 kHz, the PCSs noise can be reduced greatly and the sizes of the magnetic materials, such as a transformer and inductor, are also reduced. This makes a path to design a simple and lossless power conversion system. As a 50 kHz DAB-IBDC is preferred, a simple high power high frequency transformer was designed using a ferrite core, as shown in Figure 7, with a transform turn ratio (n) of 3:4 and a leakage inductance of 5.26 μH.
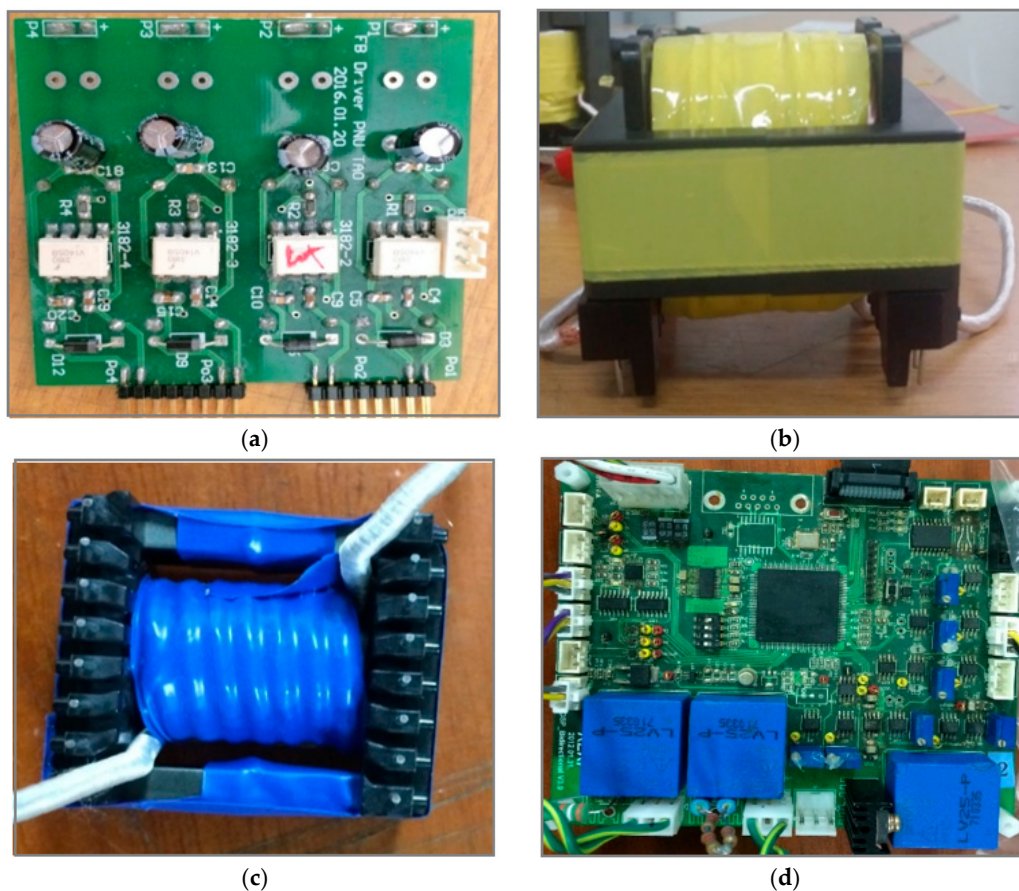

(a)	(b)

(c)	(d)

Figure 7. DAB-IBDC converter sub circuits and magnetic components. (**a**) MOSFET driving circuit; (**b**) Transformer; (**c**) Inductor; (**d**) Digital controller.

According to the DAB-IBDC design, the required inductance is 9.98 μH, which can be given by the transformer leakage inductance, either alone or combined with an external coupling inductor. As per the design, to reach the required inductance of the circuit, at the transformer secondary side, an additional inductor with a value of 4.72 μH is connected in series. The additional inductor is called the coupled inductor, and the overall inductance is called the auxiliary inductance of the circuit. Table 1 lists the developed 2 kW DAB-IBDC converter specifications. The input source of the DAB converter was a 220 V renewable solar energy DC source, which was obtained from six 38 V, 340 W solar panels connected in series. The output was connected to the supercapacitor bank, which were built with three 48 V, 165 F, and 53 Wh Maxwell supercapacitors connected in parallel. The overall supercapacitor bank specification was 48 V, 495 F, and 159 Wh. The proposed DAB-IBDC converter was controlled

by the digital control board which designed using a DSP (TMS320F28335) IC along with many sub circuits, such as short circuit protection, PWM protection, soft start, voltage sensor and current sensor which shown in Figure 7d.

Table 1. DAB-IBDC converter design specification.

Parameter	Rating
Input Voltage	200–220 V
Power	2000 W
Output Voltage	48 V
Transformer turns ratio	3:4
Switching frequency	50 kHz
Secondary leakage inductance	5.26 μH
Auxiliary inductance	4.72 μH
Input capacitor	1200 μF
Output capacitor	1800 μF

Digital Control System

A closed loop controller is required in power converters for regulating the output voltage/current and also it is needed to compensate the source/load disturbance. The closed loop controller is essentially used to minimize or eliminate the error in an output. The proposed digital control algorithm's flow chart and control loop for the DAB-IBDC converter presents in Figures 8 and 9. The four variables called the output voltage (V_{out}), input voltage (V_{in}), input current (I_{in}), and output current (I_{out}) of the DAB-IBDC converter are given to the DSP as processing variables through voltage and current sensors. LV25-P (LEM Components, Geneva, Switzerland) and LA25-P (LEM Components, Geneva, Switzerland) were used as a voltage and current sensors. These sensors sense the I/O voltages and I/O currents of the DAB-IBDC converter and sends corresponds low voltage signal to the DSP. The DSP controller operates the MOSFET switches in higher switching frequency. It generates the high frequency-50% dutycycle PWM signals for triggering MOSFET switches which located at both side bridges. Along with this, the DSP generates the inner and outer phase angle based on the proposed control algorithm, which controls the DAB-IBDC towards achieving a safe charging, maximum power point, and high efficiency power conversion. In DSP control, proportional integral (PI) controller has been used for achieving zero steady state error in an output by finding proper phase angle:

$$\text{PI controller} = K_p\, e(t) + \frac{1}{K_i} \int_0^t e(\tau)\mathrm{d}\tau \tag{17}$$

Digital PI controller is given by:

$$\text{PI\_out} = \text{Pre\_PI\_out} + \text{Err} \times (K_p + 0.5{*}K_i{*}T_s) + \text{Pre\_Err} \times (0.5{*}\, K_i \times T_s - K_p) \tag{18}$$

where Err = Ref − Variable, Pre_Err = previous Err value, Pre_PI_out = Previous PI_out value, K_p—Proportional controller gain and K_i—integral controller gain.

The proposed blended SPS-ESPS digital control algorithm initially performs the control process started with the SPS control algorithm. The controller generates an error signal based on the reference and output voltage. The voltage Proportional Integral (PI) controller process that error signal and finds the value for the outer phase shift (d). Thus, while staring, the DAB-IBDC converter inevitably sets the phase shift between the two bridges square waves V_{ab} and V_{cd} using SPS control algorithm. This helps in achieving safe charging current (Equation (3)) for the supercapacitors by controlling the inductor current (I_L). Meanwhile, the MPPT algorithm runs parallelly and continuously monitors the input power. At every cycle, it frequently varies the current reference value (I_{ref}), subsequently monitors the correspond changes in an input power. In six to ten DSP timing cycles, the algorithm finds the better reference value where the maximum input power can be obtained. The error signal

is generated by comparing this reference value with supercapacitor charging current. Current PI controller processed that error signal and generated the value which modifies phase shift '*d*' again. MPPT algorithm routinely repeating the same process parallel with SPS algorithm and finding the reference value towards continuously achieving the maximum power point at every time instants. Thus, the MPPT algorithm works in parallel with SPS control algorithm to achieve maximum power point tracking for the solar source.
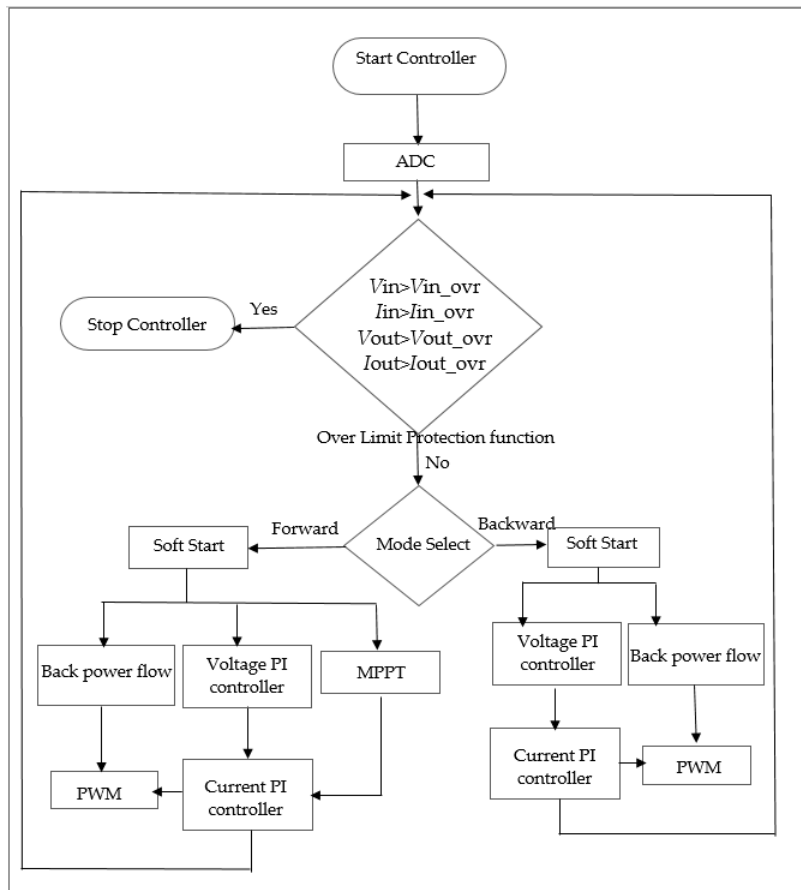

Figure 8. Blended SPS-ESPS digital control algorithm flow chart.
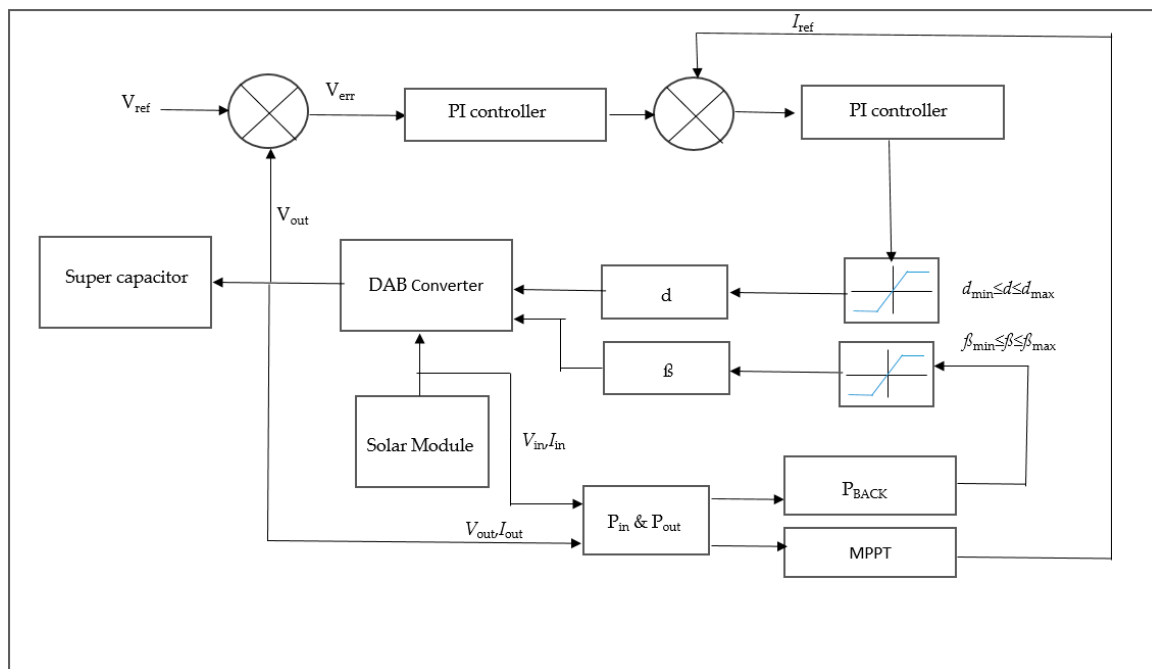
Figure 9. Blended SPS-ESPS digital control algorithm control loop.

Later ESPS control begins to analyse the back-power flow of the circuit and set the inner phase shift (β) for the primary bridge to achieve low back power flow in a circuit (Equations (14) and (15)). The ESPS region achieves the maximum possible conversion efficiency by reducing the back-flow power. The back-flow power of a circuit depends the voltage conversion ratio 'k' ($k = V_{in}/n \times V_{out}$). For large input to output voltage variations, 'k' will be greater than one. According to [21], a comparison of ESPS with the SPS control algorithm showed that SPS control DAB converter back power flow is low for a particular phase shift region, i.e., 0.41 to 0.5 for $k > 2$. At rest of that region, the ESPS control algorithm achieves higher efficiency than SPS by achieving low back flow power.

According to the mentioned DAB-IBDC design, 'k' is:

$$k = \frac{V_{in}}{nV_{out}} = \frac{200 \sim 222}{0.75 \times 48} \simeq 6$$

where k = Voltage transfer ratio.

From the Equations (6) and (15), it is noted that the back-flow power (P_{bf}) is directly proportional to the voltage transfer ratio 'k', so the back-flow power for this DAB-IBDC design also will be the maximum as it has the maximum k value. Therefore, to increase the power conversion efficiency in such a large input to output voltage variation, this paper proposed a combination of SPS and ESPS control algorithm. This works in a such a way that for a particular outer phase shift 'd' region, it will follow the SPS control algorithm and the remainder of the other phase shift 'd' region it will obey the ESPS algorithm. Thus, the proposed control algorithm operates in both SPS and ESPS mode for achieving possible maximum power conversion efficiency in a large voltage conversion ratio. When conversion is started, the proposed control algorithm initially operates the converter with a soft start algorithm to reduce the inrushing current and overshoot voltage in a circuit. Next SPS control and the MPPT algorithm are started. Parallel working of SPS control and the MPPT algorithm helps in enhancing the safety charging process for the supercapacitor bank while achieving the solar maximum power point. After that the ESPS algorithm is initiated and starts to analyze the back-flow power in a circuit. Based on this analyzation, the inner phase shift of the primary bridge is adjusted or maintaining at zero towards achieving the maximum possible power conversion efficiency. The proposed blended SPS-ESPS digital control 2 kW DAB-IBDC performance was analyzed

experimentally with a comparison study of traditional SPS digital control DAB-IBDC. Both experiment results are discussed below. The proposed control algorithm achieved better conversion efficiency than the tradition control algorithm in a large voltage conversion ratio caused renewable energy storage system.

4. Results and Discussion

Both the SPS and blended SPS-ESPS control DAB-IBDC converter power conversion performance discussed below are based on the experimental results. The experiments were conducted in a standalone renewable energy storage system with a combination of 2 kW solar modules and a 153 Wh supercapacitor bank. The experiments were conducted during different time stages towards achieving different input power and voltages by solar module. The DAB-IBDC converter output waveforms are discussed for the various input powers 2000, 1900, 1700 and 1400 W, and the circuit performance is analyzed using the experimental results. The SPS control DAB-IBDC conversion waveform, charging time, and efficiency are discussed below.

A single phase shift control is a traditional control technology for a DAB-IBDC converter. Figure 10 shows that the SPS controls the DAB-IBDC conversion waveforms for different input powers. The HV (V_{ab}) and LV (V_{cd}) side voltage, inductor current, and output charging voltage are shown for each input power from Figure 10a,b. Figure 9 shows that DSP automatically varies the phase shift (0.47 to 0.245) between V_{ab} and V_{cd} to achieve a constant output voltage and limiting current based on the SPS control algorithm. The solar source achieved an input voltage from a to d of 221.7 V, 216.3 V, 211.1 V, and 207.7 V, respectively. The SPS digital control algorithm changed only the outer phase shift to control the inductor current and obtain a constant dc output voltage.
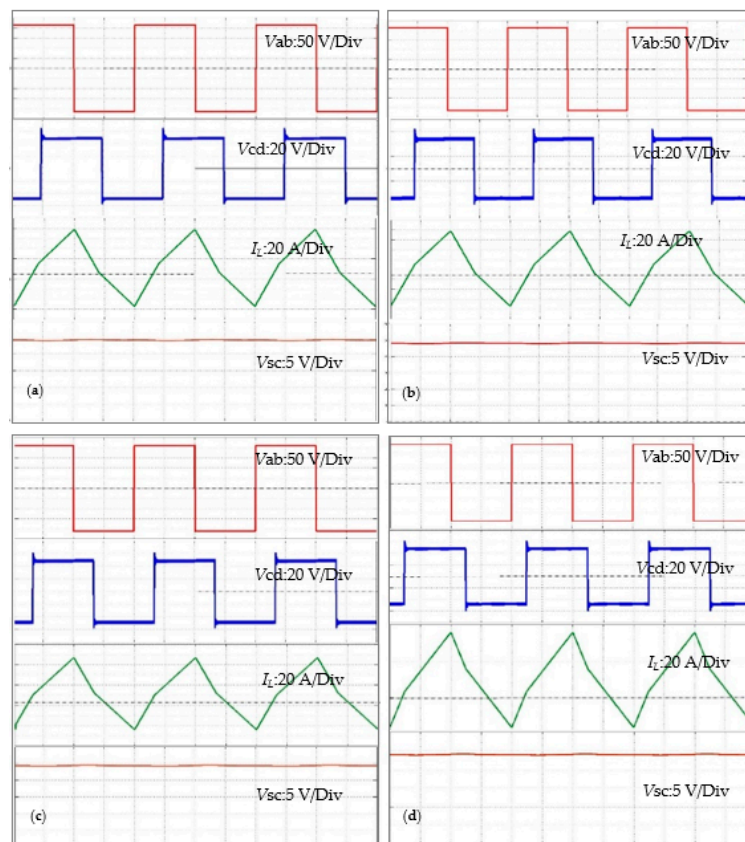

Figure 10. Experiment results of the SPS control DAB-IBDC converter at different input power (**a**) 2000 W; (**b**) 1900 W; (**c**) 1700 W and (**d**) 1400 W. Time scale: 5 ms/Div.

Figure 11 presents the super capacitor charging waveform for SPS control DAB-IBDC converter; Figure 11a shows the time vs. voltage characteristics waveforms and Figure 11b shows the time vs. current characteristics waveforms of the converter. This takes 6 min 26 s, 6 min 58 s, 7 min 43 s, and 9 min 23 s to charge a 158 Wh-supercapacitor bank with a respective input power of 2000, 1900, 1700 and 1400 W. On the other hand, according to the theoretical calculation, a 2000, 1900, 1700 and 1400 W input energy can charge a 158 Wh supercapacitor bank in 4 min 45 s, 5 min 01 s, 5 min 35 s, and 6 min 47 s, respectively. Owing to the power losses in a circuit SPS control algorithm achieves less efficiency for the given prototype. The efficiency of the converter can be calculated from the difference between the theoretical and experimental values, which are plotted in Figure 12.

Figure 12a,b shows the achieved output power and power conversion efficiency of the SPS control DAB-IBDC converter. SPS control topology achieved a power conversion efficiency of 73%, 72.6%, 71%, and 69% for an input solar power 2000 W, 1900 W, 1700 W, and 1400 W, respectively. As discussed above, the efficiency of a converter will be reduced due to backflow power in a circuit. To reduce the back-flow power in a circuit, the blended SPS-ESPS control algorithm was proposed. To compare the performance of the converter in both control algorithm, the same experiments were repeated with the same operating conditions using the blended SPS-ESPS control algorithm and experimental results are given below.

Figure 13 shows the blended SPS-ESPS control DAB-IBDC circuit waveforms. The two square wave signals S1, S4 are the switching signals for the two inner branches of the primary bridge. The phase shift between these two branches called the inner phase shift (β) controls the back-flow power in a circuit. S5,7 are the square wave switching signals for the secondary bridge. The phase shift between S1 and S5 are called the outer phase shift ratio (d), which controls the power flow in a circuit. The HV side voltage (V_{ab}) and LV side voltage (V_{cd}) are shown in the Figure 13, in which V_{ab} changes considerably due to the inner phase shift. In the figure comparing the waveform (*a*), the inner phase shift was quite large for other waveforms. As the solar input voltage decreases, the outer phase shift increases to compensate for the desired output dc voltage. Therefore, the back flow power in a circuit increases and subsequently the conversion output power of the circuit is decreased. Figure 13 shows the proposed algorithm to reduce the back-power flow by increasing the inner phase shift. Because the additional phase shift voltage difference across the inductor has six levels of changes, it resembles the changes in inductor current.
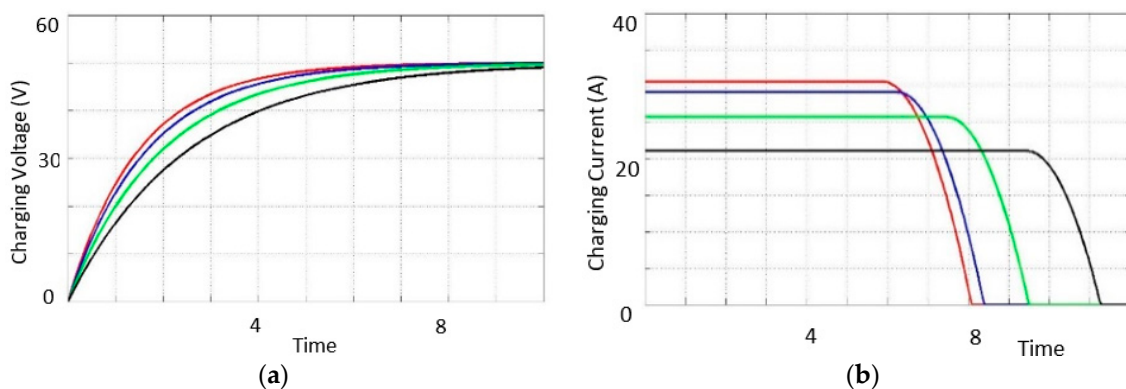

Figure 11. Supercapacitor charging waveform by SPS control DAB-IBDC converter. (**a**) Shows the time vs. voltage characteristics waveforms and (**b**) shows the time vs. current characteristics waveforms of the converter.
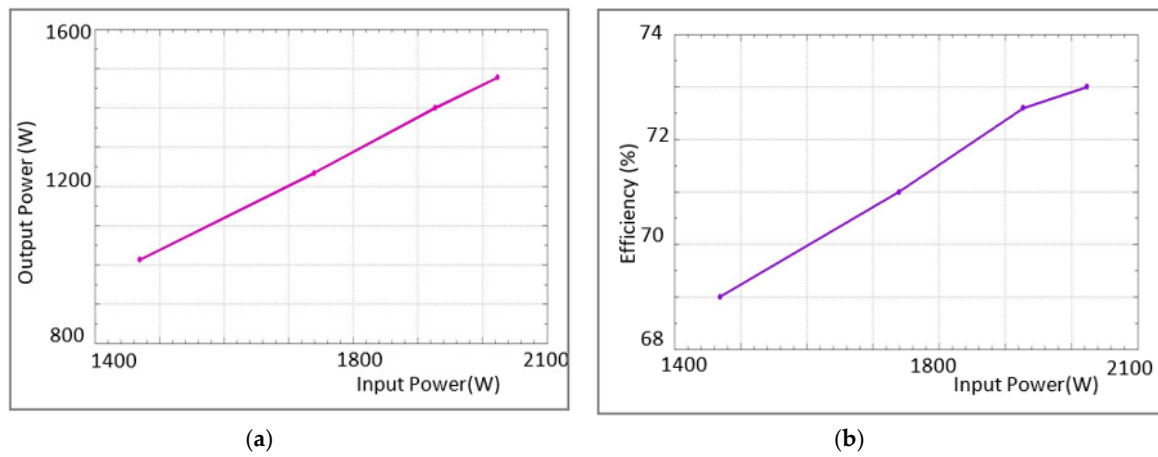
(**a**)

(**b**)

Figure 12. SPS control DAB-IBDC converter power conversion efficiency for the different input solar power. (**a**) Shows the the achieved output power of the SPS control DAB-IBDC converter and (**b**) shows the power conversion efficiency of the SPS control DAB-IBDC converter.
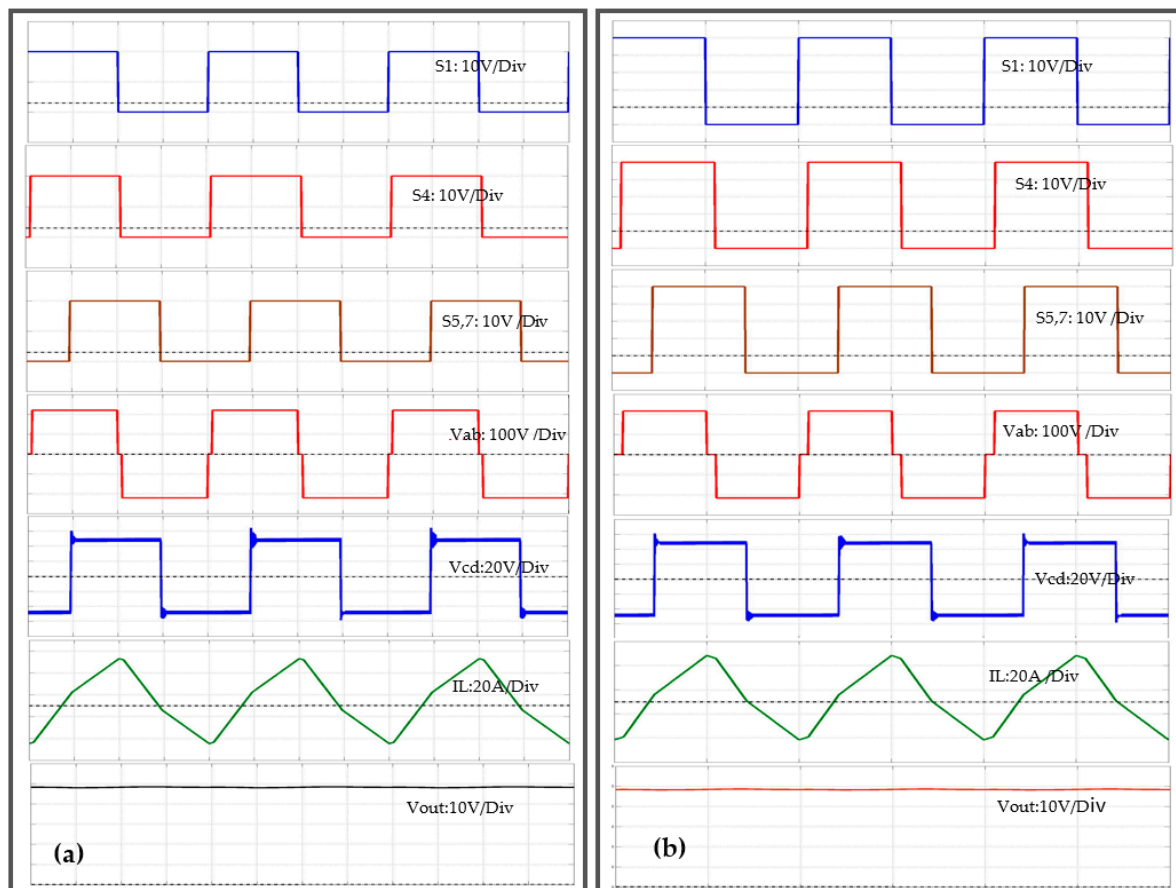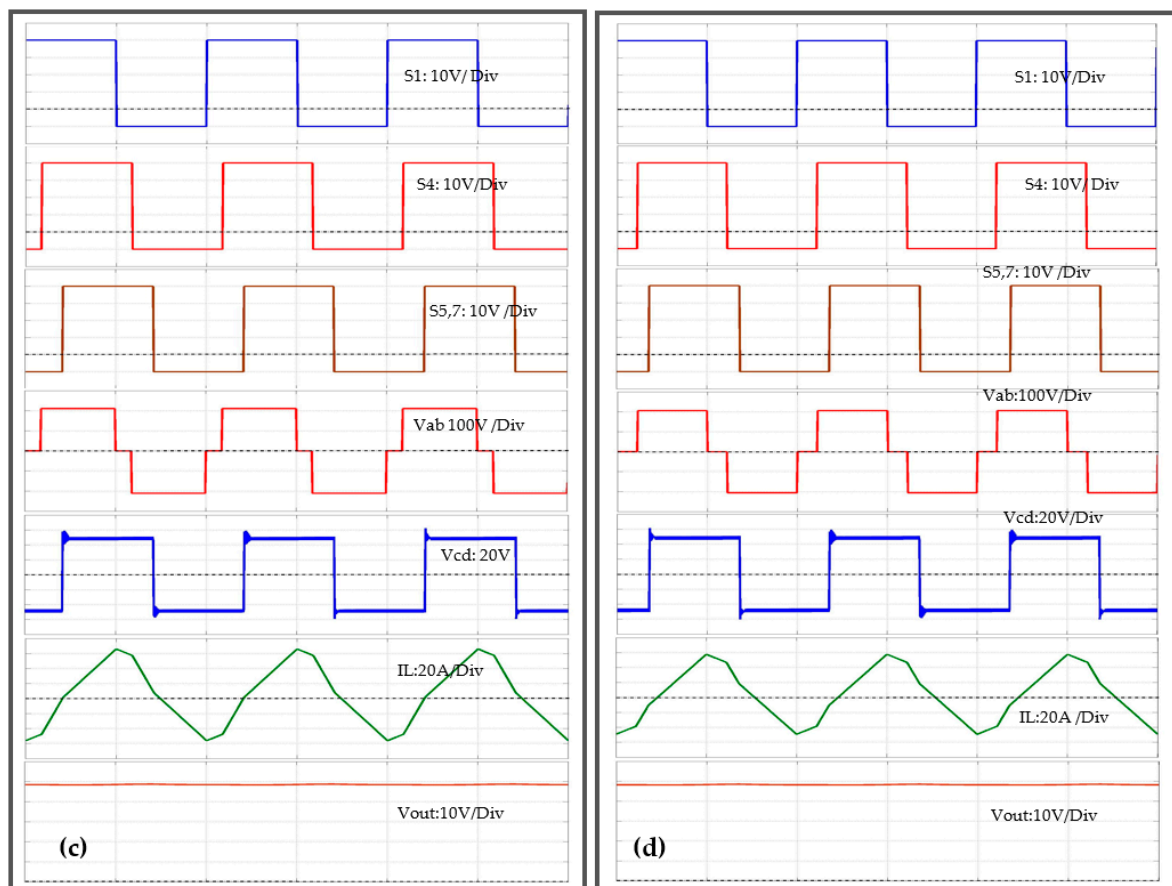

Figure 13. *Cont.*

Figure 13. Blended SPS-ESPS control DAB-IBDC conversion waveform for a different input power that (**a**) 2000 W; (**b**) 1900 W; (**c**) 1700 W and (**d**) 1400 W. Time scale 5 ms/Div.

Figure 14 shows the AC link current waveforms generated by the two active bridges. Figure 14a,b show the LV and HV side device current waveforms. From the figure, introducing an inner phase shift in a single phase shift reduces the switching reverse current or back flow power. From the measured results, the blended SPS-ESPS control converter operates with a maximum conversion efficiency of 84%.

Figure 15 presents the power conversion efficiency comparison plot for SPS and proposed control algorithm; (a) shows that the power conversion efficiency and (b) shows that achieved output power respective to various input solar powers. The blended SPS-ESPS topology achieved a power conversion efficiency of 75%, 79%, 84%, and 81% for the respective input solar power of 2000, 1900, 1700 and 1400 W. Compared to the SPS control algorithm, it increases the power conversion efficiency with 2–13% and take 6 min 14 s, 6 min 15 s, 6 min 30 s and 7 min 59 s to charge a 158 Wh-supercapacitor bank with a respective input power of 2000, 1900, 1700 and 1400 W.
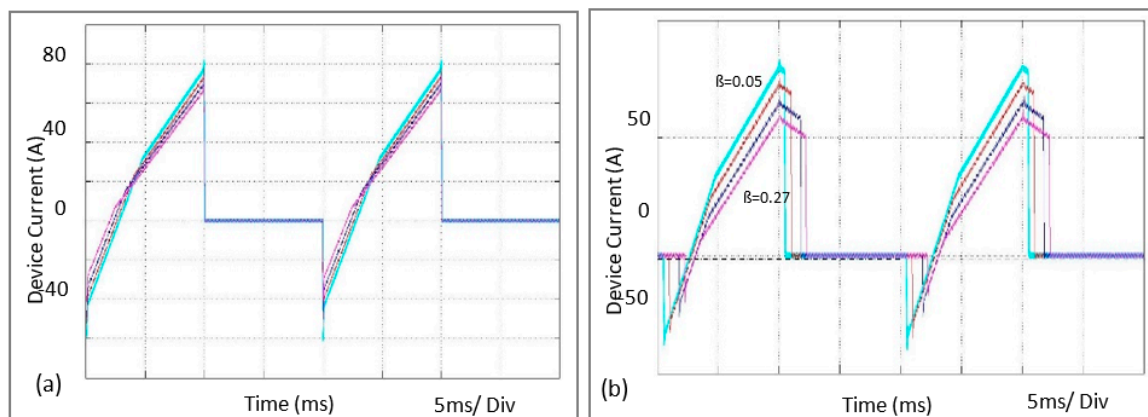
Figure 14. Experimental results of device current waveform of blended SPS-ESPS controlled DAB-IBDC converter. (**a**)Primary bridge switching current; (**b**) Secondary bridge switching current.
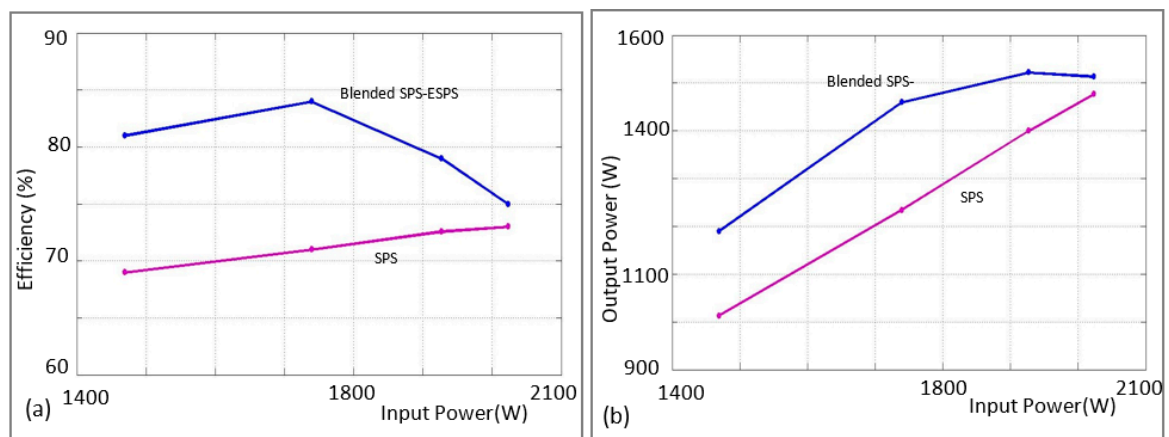

Figure 15. Blended SPS-ESPS control DAB-IBDC Power conversion efficiency. (**a**) Input Power vs. Efficiency; (**b**) Input Power vs. Output Power.

Figure 16 shows backward mode operation waveforms of SPS (a) and blended SPS-ESPS (b) control DAB-IBDC converter. At the backward mode, high power resistive load (25 Ω) was used at the primary side of the converter circuit, as shown in the block diagram which Figure 1, for discharging the supercapacitor bank. In forward mode, when the supercapacitor was fully charged, the controller automatically switched from forward mode to backward mode and enabled reverse side power flow in a circuit. In the experiment, a 25 Ω, 2500 W resistive load was connected at the primary side to discharge a 158 Wh super capacitor bank. The supercapacitor bank output voltage was 48 V, which was converted to 220 V dc at backward mode and applied across the load of 25 Ω. An approximately 9 A current was passed through the load.
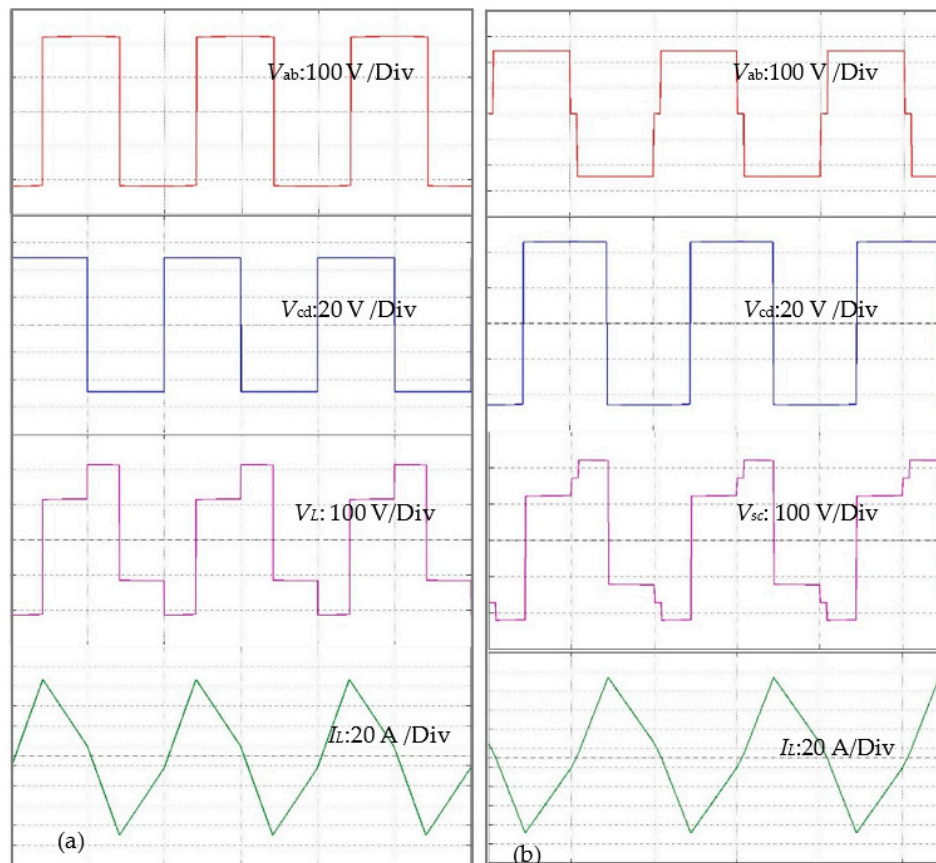
Figure 16. Backward mode operation waveforms of (**a**) SPS control; (**b**) Blended SPS-ESPS control DAB-IBDC. Time scale 10 ms/Div.

5. Conclusions

The blended SPS-ESPS digital control algorithm was proposed over the SPS control algorithm for a DAB-IBDC converter to achieve a high-power conversion efficiency, maximum power point, and enhanced fast charging-discharging in a high power density energy storage device. In the laboratory, using MOSFET switches, a 2 kW, 50 kHz DAB-IBDC converter was developed and the SPS and a blended SPS-ESPS control algorithm were verified experimentally. The results showed that in large voltage conversion ratio applications, such as a standalone solar power systems, the proposed blended SPS-ESPS control algorithm achieves high conversion efficiency by reducing the back-flow power and current stress in a circuit.

Author Contributions: P. Sathishkumar, Hee-Je Kim and Cheewoo Lee conceptualize the idea of this research project. P. Sathishkumar designed the DAB-IBDC converter, MOSFET driver and power units. Dong-Keun Jeong designed a DSP controller board. P. Sathishkumar and Shengxu Piao developed the control algorithm and DSP program with help of and Dong-Keun Jeong. P. Sathishkumar, Himanshu and Muhammad Adil Khan developed a magnetic component for the circuits that high frequency transformer and inductor. P. Sathishkumar, Do-Hyun Kim and Min-Soo Kim making an experimental setup and doing experiment. The data was analyzed by the team and the paper was written by P. Sathishkumar and Hee-Je Kim.

Conflicts of Interest: The authors declare no conflict of interest.

References

1.   Romano, R.; Siano, P.; Acone, M.; Loia, V. Combined operation of electrical loads, Air conditioning and Photovoltaic Battery Systems in smart houses. *Appl. Sci.* **2017**, *7*, 525. [CrossRef]

2. Khan, M.A.; Ko, B.; Alois Nyari, E.; Park, S.E.; Kim, H.-J. Performance Evaluation of Photovoltaic Solar System with Different Cooling Methods and a Bi-Reflector PV System (BRPVS): An Experimental Study and Comparative Analysis. *Energies* **2017**, *10*, 826. [CrossRef]

3. Daowd, M.; Antoine, M.; Omar, N.; Lataire, P.; van den Bossche, P.; van Mierlo, J. Battery management system—Balancing modularization based on a single switched capacitor and bi-directional DC/DC converter with the auxiliary battery. *Energies* **2014**, *7*, 2897–2937. [CrossRef]

4. Xiang, C.; Wang, Y.; Hu, S.; Wang, W. A new topology and control strategy for a hybrid battery-ultracapacitor energy storage system. *Energies* **2014**, *7*, 2874–2896. [CrossRef]

5. Sheldon, S.W. Electric and Plug-in Hybrid Electric Vehicle Drive Train Topologies. In *Energy Management Strategies for Electric and Plug-in Hybrid Electric Vehicle*; Springer: New York, NY, USA, 2013; pp. 7–14.

6. Balamuralitharan, B.; Karthick, S.N.; Balasingam, S.K.; Hemalatha, K.V.; Selvam, S.; Anandha Raj, J.; Prabakar, K.; Jun, Y.; Kim, H.-J. Hybrid Reduced Graphene Oxide/Manganese Diselenide Cubes: A New Electrode Material for Supercapacitors. *Energy Technol.* **2017**. [CrossRef]

7. Lai, C.M.; Lin, Y.C.; Lee, D.S. Study and implementation of a two-phase interleaved bidirectional DC/DCconverter for vehicle and dc-microgrid systems. *Energies* **2015**, *8*, 9969–9991. [CrossRef]

8. Tsai, C.-T.; Chen, W.-M. Buck converter with soft switching cells for PV panel applications. *Energies* **2016**, *9*, 148. [CrossRef]

9. Patel, H.; Agarwal, V. MPPT Scheme for a PV-Fed Single-Phase Single-Stage Grid-Connected Inverter Operating in CCM with Only One Current Sensor. *IEEE Trans. Energy Convers.* **2009**, *24*, 256–263. [CrossRef]

10. Hsieh, Y.P.; Chen, J.-F.; Yang, L.-S.; Wu, C.-Y.; Liu, W.-S. High-conversion-ratio bidirectional DC-DC converter with coupled inductor. *IEEE Trans. Ind. Electron.* **2014**, *61*, 210–222. [CrossRef]

11. De Doncker, R.W.A.A.; Divan, D.M.; Kheraluwala, M.H. A three-phase soft-switched high-power-density dc/dc converter for high-power applications. *IEEE Trans. Ind. Appl.* **1991**, *27*, 63–73. [CrossRef]

12. Biela, J.; Schweizer, M.; Waffler, S.; Kolar, W.J. SiC versus Si—Evaluation of potentials for performance improvement of inverter and dc-dc converter systems by SiC power semiconductors. *IEEE Trans. Ind. Electron.* **2011**, *58*, 2872–2882. [CrossRef]

13. Alonso, A.R.; Sebastian, J.; Lamar, D.G.; Hemando, M.M.; Vazquez, A. An overall study of a Dual Active Bridge for bidirectional DC/DC conversion. In Proceedings of the 2010 IEEE Energy Conversion Congress and Exposition (ECCE), Atlanta, GA, USA, 12–16 September 2010. [CrossRef]

14. Zhao, B.; Song, Q.; Liu, W.; Sun, Y. Overview of Dual-Active-Bridge Isolated Bidirectionla DC-DC Converter for High-Frequency-Link power conversion system. *IEEE Trans. Power Electron.* **2014**, *29*, 4091–4106. [CrossRef]

15. Naayagi, R.T.; Andrew, J.; Shuttleworth, R. High-Power bidirectional DC-DC converter for Aerospace applications. *IEEE Trans. Power Electron.* **2012**, *27*, 4366–4379. [CrossRef]

16. Jeong, D.-K.; Ryu, M.-H.; Kim, H.-G.; Kim, H.-J. Optimized design of bidirectional dual active bridge converter for low voltage battery charger. *J. Power Electron.* **2014**, *14*. [CrossRef]

17. Inoue, S.; Akagi, H. A bidirectional isolated dc-dc converter as a core circuit of the next-generation medium-voltage power conversion system. *IEEE Trans. Power Electron.* **2007**, *22*, 535–542. [CrossRef]

18. Zhou, H.; Khambadkone, A.M. Hybrid modulation for dual active bridge bi-directional converter with extended power range for ultracapacitor application. *IEEE Trans. Ind. Appl.* **2009**, *45*, 1434–1442. [CrossRef]

19. Naayagi, R.T.; Forsyth, A.J.; Shuttleworth, R. Performance analysis of extended phase shift control of DAB DC-DC converter for Aerospace energy storage system. In Proceedings of the 2015 IEEE 11th International Conference on Power Electronics and Drive Systems (PEDS), Sydney, Australia, 9–12 June 2015.

20. Zhao, B.; Yu, Q.; Sun, W. Extended-Phase shift control of isolated bidirectional dc-dc converter for power distribution in microgrid. *IEEE Trans. Power Electron.* **2012**, *27*, 4667–4680. [CrossRef]

21. Shi, X.; Jiang, J.; Guo, X. An efficiency-optimized isolated bidirectional dc-dc converter with extended power range for energy storage systems in microgrids. *Energies* **2013**, *6*, 27–44. [CrossRef]